JVSTA Journal of Vacuum Science & Technology A

Molecular beam epitaxial growth and scanning tunneling microscopy studies of the gallium rich trench line structure on N-polar w-GaN(000 1 ¯)

Zakia H. Alhashem, Andrada-Oana Mandru, Jeongihm Pak, and Arthur R. Smith

Citation: Journal of Vacuum Science & Technology A **33**, 061404 (2015); doi: 10.1116/1.4927163
View online: http://dx.doi.org/10.1116/1.4927163
View Table of Contents: http://scitation.aip.org/content/avs/journal/jvsta/33/6?ver=pdfcov
Published by the AVS: Science & Technology of Materials, Interfaces, and Processing

Molecular beam epitaxial growth and scanning tunneling microscopy studies of the gallium rich trench line structure on N-polar *w*-GaN(000$\bar{1}$)

Zakia H. Alhashem, Andrada-Oana Mandru, Jeongihm Pak, and Arthur R. Smith[a)]
Nanoscale and Quantum Phenomena Institute, Department of Physics and Astronomy, Ohio University, Athens, Ohio 45701

(Received 13 April 2015; accepted 8 July 2015; published 24 July 2015)

In addition to the usual set of the well-known reconstructions that have been observed on the N-polar GaN surface, namely 1×1, 3×3, 6×6, and c(6×12), an additional structure is occasionally seen at high Ga coverage, which can extend over a large area of the surface. This structure, which is referred to as trench line structure, is partially ordered and consists of parallel-running dark (trench) lines separating wide and narrow strips of atomically ordered regions. There are also randomly placed defects interrupting the ideal ordering. Reflection high energy electron diffraction and scanning tunneling microscopy in ultrahigh vacuum are applied to investigate this trench line structure on samples prepared using molecular beam epitaxy. It is found that the trench line structure results from annealing the Ga-rich c(6×12) at high temperature followed by quenching to room temperature. By careful comparison of the scanning tunneling microscopy images with those from neighboring c(6×12) regions, it is found that the trench line structure can be decomposed into subunits of the c(6×12). Using these subunits, some simple models for the trench line structure are created. It is proposed that the trench line structure is composed of two primary c(6×12) subunits consisting of first and second layer Ga adatoms and that the trench lines are regions devoid of Ga adatoms, going down to the Ga adlayer. © *2015 American Vacuum Society*. [http://dx.doi.org/10.1116/1.4927163]

I. INTRODUCTION

Gallium nitride (GaN) is a well-known semiconducting material, which is widely used in a variety of electronic applications due to its unique and important properties. One of its unique qualities is that the wide band gap of GaN (3.4 eV) gives rise to widespread optoelectronic applications such as blue light emitting diodes and lasers.[1,2] GaN is a binary III/V semiconducting material, which has a direct band gap. It has a wurtzite (similar to hexagonal) crystal structure that can be grown with one of two different basal plane polarities, which is determined by the bond directions of the N (or Ga) atoms.[3] The gallium polar (Ga-polar) GaN (0001) surface has one Ga bond up and three Ga bonds down. Oppositely, the nitrogen polar (N-polar) GaN(000$\bar{1}$) surface has one N bond up and three N bonds down.

In 1997, Smith *et al.* observed four dominant reconstructions on the N-polar GaN(000$\bar{1}$) surface: 1×1, 3×3, 6×6, and c(6×12) in order of increasing Ga/N stoichiometry.[4] These four reconstructions were prepared using molecular beam epitaxy (MBE) and studied at room temperature using scanning tunneling microscopy (STM) as well as reflection high energy electron diffraction (RHEED). On the other hand, the Ga-polar GaN(0001) surface has four completely different reconstructions, which were also reported by Smith *et al.* in 1998. These Ga-polar structures include 2×2, 5×5, 6×4, and "1×1" in order of increasing Ga/N stoichiometry.[5,6] Most of these structures, on both polarities, are stabilized under Ga-rich conditions, a point which remains of considerable practical as well as theoretical interest.[7,8]

Since the discovery of the different reconstructions on GaN surfaces, considerable attention has been devoted to improving GaN growth for semiconductor applications. At the same time, spin injection of a ferromagnetic material into a semiconducting material has been of increasing interest, leading to important spintronic applications.[9,10] It is pretty clear that the starting surface reconstruction can play a role in subsequent magnetic film growth and properties. This has been seen, for example, in the case of GaAs surfaces, in which it has been debated how the starting surface reconstruction could affect the magnetic anisotropy of overgrown Fe layers.[11,12] For GaN surfaces, there has been quite a bit of interest in the overgrowth of magnetic layers as well, and detailed studies have found a variety of reconstructions at the initial stages of transition metal growth on clean GaN surfaces.[13,14] One paper recently discussed the importance of N-polar GaN surfaces for achieving particular cube-on-hexagon orientation relationships for overgrown Fe layers.[15]

In 2012, Chinchore *et al.* deposited Mn atoms on the Ga-rich GaN(000$\bar{1}$) surface which led to the formation of two-dimensional atomically smooth MnGa islands with heights close to 1 nm.[16] MnGa is a well-known ferromagnetic Heusler family compound, which exhibits perpendicular magnetic anisotropy (PMA) in thin film layers.[17] Materials exhibiting PMA are of very high interest for applications such as spin-transfer-torque magnetic random access memories.[18] The key to forming these unique quantum height MnGa islands is that the starting surface reconstruction prior to Mn deposition should consist of a network of trench line structures. In the paper by Chinchore *et al.*, these structures were observed and shown in regions between the MnGa islands. The nanometer high MnGa islands do not form well on other starting

[a)]Author to whom correspondence should be addressed; electronic mail: smitha2@ohio.edu

reconstructions such as the 3×3 or $c(6 \times 12)$. This is therefore a very important and not understood surface reconstruction.

The trench line structures are reminiscent of the $2 \times n$ vacancy line structures, which are well-documented to occur on Si(001) surfaces which normally have the 2×1 dimer reconstruction.[19,20] While ascribed by many to be evidence of Ni contamination, Martin and co-workers found little evidence for Ni on the thermally quenched $2 \times n$ surface.[21] In 1995, Smith *et al*. found that high temperature annealing and quenching the Si(001) surface down to room temperature led to the formation of vacancy chains that became vacancy lines after further annealing and quenching.[22,23] Smith *et al*. believed that the cause of the $2 \times n$ vacancy line structure was an interaction between dimer vacancy clusters.

This paper presents an initial investigation of the trench line structure (TLS) on N-polar GaN($000\bar{1}$). A method of preparing the structures is determined and presented here. Similar to the case of the Si(001) $2 \times n$ vacancy line reconstruction, we find that the TLS is formed by high temperature annealing and quenching of the $c(6 \times 12)$ reconstruction. STM images of the TLS are presented along with $c(6 \times 12)$, and finally, some starting point models for the TLS are proposed based on comparison of the structural subunits to those of the $c(6 \times 12)$ reconstruction.

II. EXPERIMENTAL PROCEDURE

GaN samples were grown on sapphire(0001) substrates using ultrahigh vacuum MBE. The growth was monitored using a RHEED system. For room temperature STM studies, the samples were transferred *in-situ* to the analysis chamber, where images were taken using a tungsten (W) tip under constant current conditions. The growth process was under highly Ga-rich conditions.[4] The heteroepitaxy process[24,25] was applied in the current experiment by growing the GaN sample on a sapphire(0001) substrate with size of $1.0\,\text{cm} \times 1.0\,\text{cm}$. The substrate was back coated with titanium (Ti) in order to be uniformly heated.

Initially, the substrate was cleaned using acetone and isopropanol alcohol, and then introduced into the MBE growth chamber. Inside the chamber, where the base pressure was $\sim 1.3 \times 10^{-10}$ Torr, the sapphire substrate was annealed at $\sim 1000\,^{\circ}\text{C}$ and simultaneously nitrided for ~ 30 min under running radio frequency nitrogen plasma. The nitrogen plasma source is a radio frequency source by SVTA and is operated at a forward power setting of ~ 450 W and a reverse power of ~ 2 W, while the background N_2 pressure is normally about 2×10^{-5} Torr. The purpose of this annealing/nitridation step was to remove surface contaminants and nitridate the sapphire surface in order to promote N-polar GaN growth.

Following this step, a GaN buffer layer was grown for ~ 7 min after lowering the substrate temperature to $\sim 665\,^{\circ}\text{C}$. In order to grow this buffer layer, the Ga effusion cell temperature was increased to $1060\,^{\circ}\text{C}$, and then, the cell was opened while the N plasma was running. The Ga flux was ~ 1–3×10^{14} atoms/cm^2/s (equal to 0.088–0.26 ML/s, where 1 ML for GaN is $\sim 1.135 \times 10^{15}$ atoms/cm^2), resulting in Ga-rich growth conditions, which is known for producing smooth GaN growth. The next step was growing the main layer of N-polar GaN for ~ 90 min. During this period of time, the sample was heated to a higher temperature (within a range of $\sim 670\,^{\circ}\text{C}$ up to $\sim 790\,^{\circ}\text{C}$), the Ga cell temperature was increased from $\sim 1080\,^{\circ}\text{C}$ up to $1110\,^{\circ}\text{C}$, while the pressure inside the growth chamber was maintained at $\sim 1.8 \times 10^{-5}$ Torr. The film was grown to a thickness of ~ 200 nm, far above the critical thickness for strain relaxation; and we have not investigated, nor observed, any effect of the exact film thickness on the TLS formation.

The GaN growth was stopped by closing the Ga shutter and turning the N plasma off. The growth stage was cooled until it reached room temperature. As the sample cooled, the RHEED pattern showed $1\times$, $3\times$, and finally $6\times$ streaks, each observed at different temperatures, as the $c(6 \times 12)$ reconstruction formed.

In order to produce the trench line structure, the sample was annealed at $\sim 800\,^{\circ}\text{C}$ for ~ 6 min. During the annealing process, the $3\times$ and $6\times$ lines disappeared, and only $1\times$ remained. After that, the sample temperature was lowered again to $\sim 130\,^{\circ}\text{C}$ where the $3\times$ and $6\times$ streaks reappeared.

III. RESULTS AND ANALYSIS FOR THE TRENCH LINE STRUCTURE BY RHEED AND STM

Figure 1 shows the RHEED patterns for the sample prepared with the trench line structure. This sample was grown by MBE, cooled, annealed to high temperature, then cooled again, and shows either a 1×1 or $c(6 \times 12)$ reconstruction on the N-polar GaN surface depending on the temperature. Figure 1(a) shows the GaN surface just after MBE growth with a 1×1 structure, which is typical at a temperature near $750\,^{\circ}\text{C}$. Upon cooling as shown in Fig. 1(b), the RHEED pattern transforms to that for a $c(6 \times 12)$ reconstruction, which consists of 1/3rd order and faint 1/6th order streaks in addition to the main first order streaks. Upon high temperature annealing as shown in Fig. 1(c), the RHEED pattern shows just the 1×1 structure. Finally, upon cooling back down, the RHEED shows again the $c(6 \times 12)$ reconstruction. No obvious noticeable change in the $c(6 \times 12)$ RHEED pattern is visible after high temperature annealing. However, as shall be shown, this surface contains large regions of TLS.

Figure 1(e) shows an STM image presented in three-dimensional perspective view of the sample surface after high temperature annealing and cooling to room temperature. As can be clearly seen, the image area contains two atomic height steps separating terraces of different structures. The well-ordered $c(6 \times 12)$ reconstruction is easily visible on the top and middle terraces.

While the $c(6 \times 12)$ reconstruction is clearly visible, also seen within the middle terrace is a region of TLS. This TLS is definitely less well-ordered compared to the $c(6 \times 12)$ regions. However, it is not a random structure, but it has a distinct characteristic appearance, which makes it stand out against the $c(6 \times 12)$. The TLS is found in this image area near the step edges of both the middle terrace and the upper

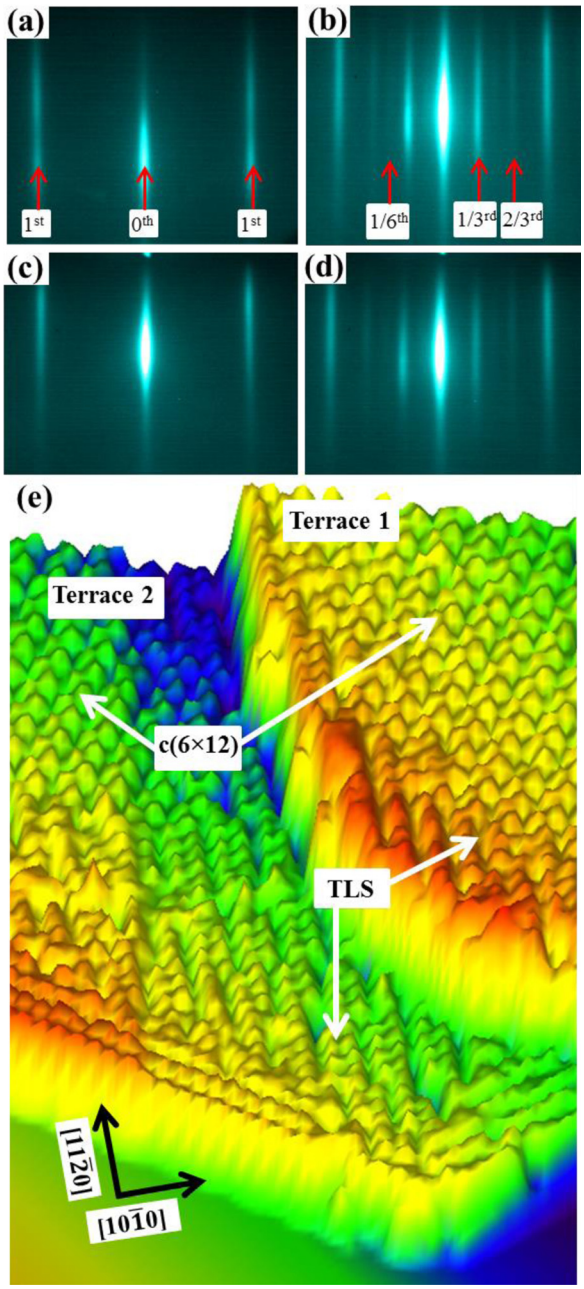

FIG. 1. (Color online) RHEED patterns corresponding to preparation of the TLS (trench line structure) with 3D perspective view STM image. (a) High temperature (757 °C) just after MBE growth showing 1×1 structure; (b) after cooling for 24 min to 186 °C showing the c(6×12) pattern; (c) at high temperature (800 °C) following 6 min of annealing and showing a 1×1 pattern; (d) after cooling for 29 min down to 129 °C showing the c(6×12) pattern; (e) 3D perspective view STM image of the surface showing both c(6×12) and TLS regions. Sample bias $V_S = -2.0$ V and tunnel current $I_T = 58.0$ pA, scanned at 200 nm/s.

terrace. It is interesting to note that in the Si(001) case, coexistence of 2×1 and $2 \times n$ structures was found on the same surface in different areas.[26]

Shown in Fig. 2(a) is a large area STM image of the sample surface, which contains both a region of c(6×12) and also a large region of TLS which are separated by the solid white line. As can be seen, these two structures blend seamlessly from one region to the other. From the c(6×12), which has a very well-known structural model (shown in Fig. 4), we can determine the crystal spacing calibration as well as the crystal lattice directions. The calibration scaling of the image can be known to high accuracy, and then it is possible to measure carefully the features seen in the TLS. For example, consider the high magnification STM image of the c(6×12) reconstruction shown in Fig. 2(b). From the unit cell, we can know the exact spacing calibration and also crystal vector directions. The unit cell has size $6 \times (3.19\,\text{Å}) = 19.1\,\text{Å}$ along the short side and $12 \times (3.19\,\text{Å}) = 38.3\,\text{Å}$ along the long side. Both sides are the high symmetry [11$\bar{2}$0] vector directions, and thus, the angles (acute and obtuse) are 60° and 120°, respectively, in this unit cell.

The TLS may be described as a partially ordered reconstruction, which contains certain well recognizable features such as the observed strips of atoms which are separated by what may be referred to as trench lines (TLs). These TLs are the dark lines while the strips have periodic rows of bright atomic features and come in two primary widths, which can be referred to as narrow strip (NS) and wide strip (WS). These are clearly seen and labeled in Fig. 2(c). The NSs and WSs are fairly well intermixed, although in some areas the WSs appear bunched together and in other areas, the NSs appear bunched together. Based on the scale calibration, we find that the WSs and NSs have widths of 9×, and 6× the GaN lattice spacing along the [10$\bar{1}$0] direction (2.76 Å), respectively. Therefore, their widths are ~24.8 Å and 16.6 Å, respectively.

Also, as characteristic features with the TLS, one can see dark rectangular shaped defects (RSDs) scattered around, which typically form at the point where a WS and an NS come together [see also Fig. 2(c)]. Corresponding also to the strip bunching, a higher density of these RSDs is seen in some areas (such as the center of the image), which also corresponds to regions with a high density of NSs. The region above the center of the image has fewer RSDs and also a higher density of WSs. So, the surface is definitely not uniform, having spatial variations on a length scale of ~10 nm.

The RSDs are not all having the same areal size; the typical ones being square shaped, and larger ones more elongated (rectangular shaped). Similar defects are occasionally found with other shapes [see near the bottom of the image of Fig. 2(a)]. These defects are clearly composed of vacancies of atoms, and as discussed further below, these are first and second layer Ga adatom vacancies. From the Ga adatom density of ~2.93 adatoms/nm^2, and the typical RSD size of ~2 nm^2, we find the typical RSD corresponds to ~6 missing Ga adatoms. The longer rectangular shaped ones could easily contain up to 12 missing adatoms.

A final observation we can make about the RSDs is that these features are chiral if we consider the terminating 2 TL's points of attachment as always offset at opposite corners of the RSD. We notice that the resulting features shown in Fig. 2(a) almost all have the same sense of chiral rotation, for example, counter-clockwise, showing that the TLS must be a chiral structure, similar to the c(6×12).[28]

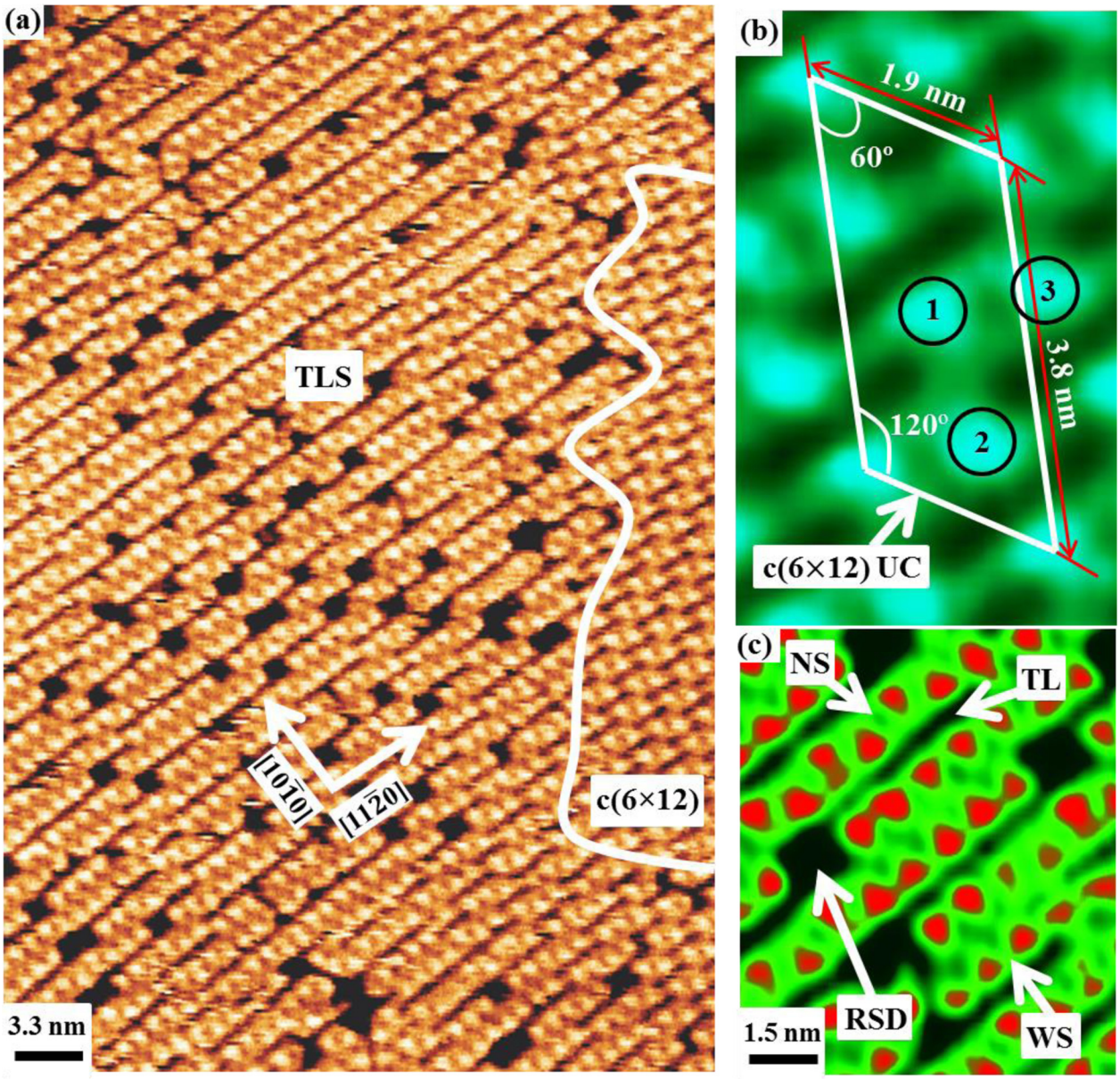

FIG. 2. (Color online) (a) Large area STM image of GaN surface with TLS (trench line structure) and c(6 × 12) regions, separated by solid white line; (b) zoom-in image of c(6 × 12) with UC (unit cell) and side lengths and angles labeled; (c) zoom-in of TLS region showing the WS (wide strip) and NS (narrow strip) features separated by TL (trench lines) and as well the RSD (rectangular shaped defect) features. Bias voltage $V_S = -1.5$ V, tunnel current $I_T = 36.6$ pA, and scanning speed = 120 nm/s.

From the zoom-in view of the c(6 × 12) reconstruction shown in Fig. 2(b), we get not only scale and crystal orientation, but also insight into the nature of the TLS. For example, we can already see that the c(6 × 12) itself contains the same TL features similar to that of the TLS area, only with a fixed and repeating length. These TLs orient in exactly the same direction as the TLs of the TLS region, namely, in the high symmetry [11$\bar{2}$0] direction. Also, the bright atomiclike features of the c(6 × 12) structure have certain characteristic spacings, which are the same as the spacings of bright features within the TLS region.

The first characteristic spacing is the spacing from the center atom within the c(6 × 12) unit cell [labeled atom 1 in Fig. 2(b)] to the off-center atom [labeled atom 2 in Fig. 2(b)], which measures 15.0 Å and which corresponds in the TLS to the spacing of bright atoms across the WS. The second characteristic spacing is the spacing from the center atom (labeled atom 1) to the nearest long edge atom [labeled atom 3 in Fig. 2(b)], which measures 11.0 Å and which corresponds in the TLS to the spacing of bright atoms across the NS. These characteristic spacings are keys to identifying models for the WS and NS structures.

The direct measurement of the characteristic spacings within the TLS is presented in Fig. 3, which shows a region of TLS and various line profiles measured across the calibrated image. The first line profile shown in Fig. 3(b) is the

line along the direction of the TLs, which is the same as [11$\bar{2}$0]. This line profile, labeled LP1, shows a corrugation amplitude of about 0.2–0.3 Å and has the repeating spacing of 9.6 Å or 3×a with $a = 3.19$ Å being the c-plane lattice parameter of GaN. The 3× periodicity along this direction is consistent with the 3× streaks seen in the RHEED pattern at room temperature.

Measuring in a direction almost (but not quite) orthogonal to [11$\bar{2}$0], we obtain the line profile LP2 cutting across the TLs and obtain two characteristic distances, as shown in Fig. 3(c). The first is a spacing of the bright features in two adjacent WSs, which measures 11.0 Å, while the second is the spacing of the bright features within a given WS and measures 15.0 Å. The corrugation amplitude for LP2 varies from 0.6 to 0.7 Å, three times greater than for LP1 and dependent upon whether it is crossing or within WSs.

The atomic corrugations of bright feature atoms within the WSs (~0.6 Å) are consistent with the corrugations corresponding to Ga adatoms. The characteristic spacing of the atoms within a single WS, being 15.0 Å, agrees exactly with the characteristic spacing of atoms [atoms labeled 1 and 2 in Fig. 2(b)] within the c(6 × 12). It is therefore possible to identify this type of atomic pair as a characteristic feature of the structure.

Measuring along the same direction as for LP2, line profile LP3 reveals similar spacings and also cuts across one of the RSDs [see lower left corner of the image shown in Fig. 3(a)]. The depth measured here is around 2.3 Å, much more than the corrugation height for just the first layer Ga adatoms, and therefore corresponds with the height of both first and second layer Ga adatoms. The bottom of the RSD, as well as the trench lines, is therefore at the level of the Ga adlayer.

From the line profiles LP2 and LP3, we also get the WS trench line spacing, which is just the sum (11.0 + 15.0 Å) that equals 26.0 Å; a comparison to the TLS spacing (25.5 Å) in the c(6 × 12) shows good agreement, further confirming the characteristic features of the WSs.

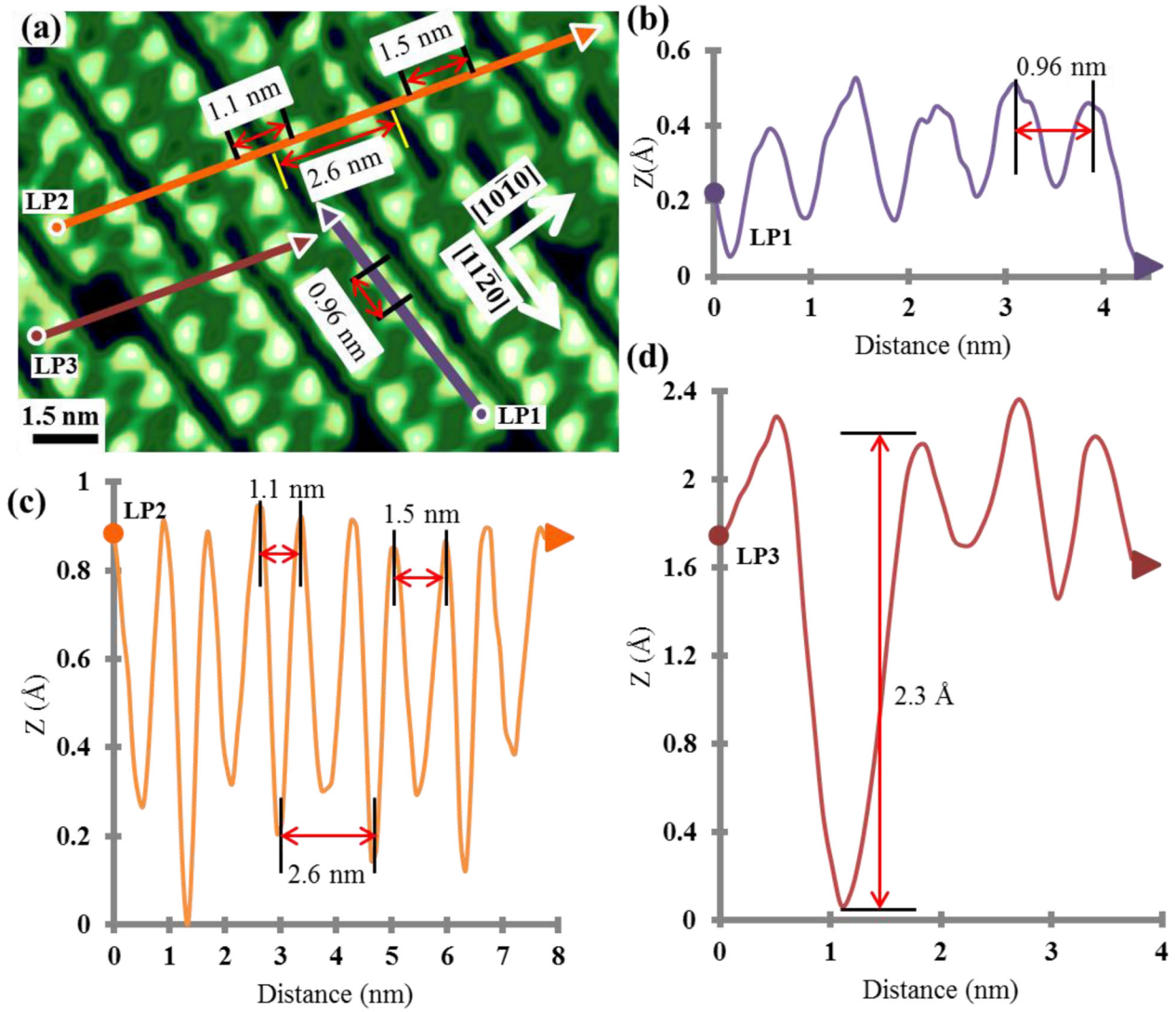

FIG. 3. (Color online) (a) STM image of the TLS on GaN (000$\bar{1}$); (b) the line profile LP1, in the [10$\bar{1}$0] direction; (c) and (d) the line profiles LP2 and LP3 in the [11$\bar{2}$0] direction. Sample bias $V_S = -1.5$ V, tunnel current $I_T = 36.6$ pA, and scanning speed = 120 nm/s.

IV. SIMPLE MODELS FOR THE TRENCH LINE STRUCTURE

In order to come up with simple models for the WS and NS within the TLS, we take advantage of the characteristic features and characteristic spacings determined using Figs. 2 and 3, and we then examine carefully the model for the c(6 × 12) reconstruction, which is presented in Fig. 4. Shown in Figs. 4(a) and 4(b) are the detailed atomic top view and side view models for the c(6 × 12), respectively, based on previous publications by Smith *et al.* and Alam *et al.*[27,28] Shown in Fig. 4(c) is an atomically resolved STM image of the c(6 × 12). It is seen by comparing the STM image features to the model that all of the bright spots in the STM image correspond to Ga trimers in which a first-layer Ga adatom sits atop two second-layer Ga adatoms in a bridge site, with the second layer Ga adatoms resting on the Ga adlayer beneath. Also shown are two additional features of the model, which correspond to features of the STM image. One feature is the c(6 × 12) TL structure shown in the model corresponding to the dark lines seen in the STM image which run along [11$\bar{2}$0]. A second feature is another second layer Ga adatom located at a hollow site within each unit cell, which was recently identified in STM images of the c(6 × 12) taken at liquid helium temperatures.[28] These correspond to a region of atomic density within the STM image and are seen clearly at certain biases at low temperature.

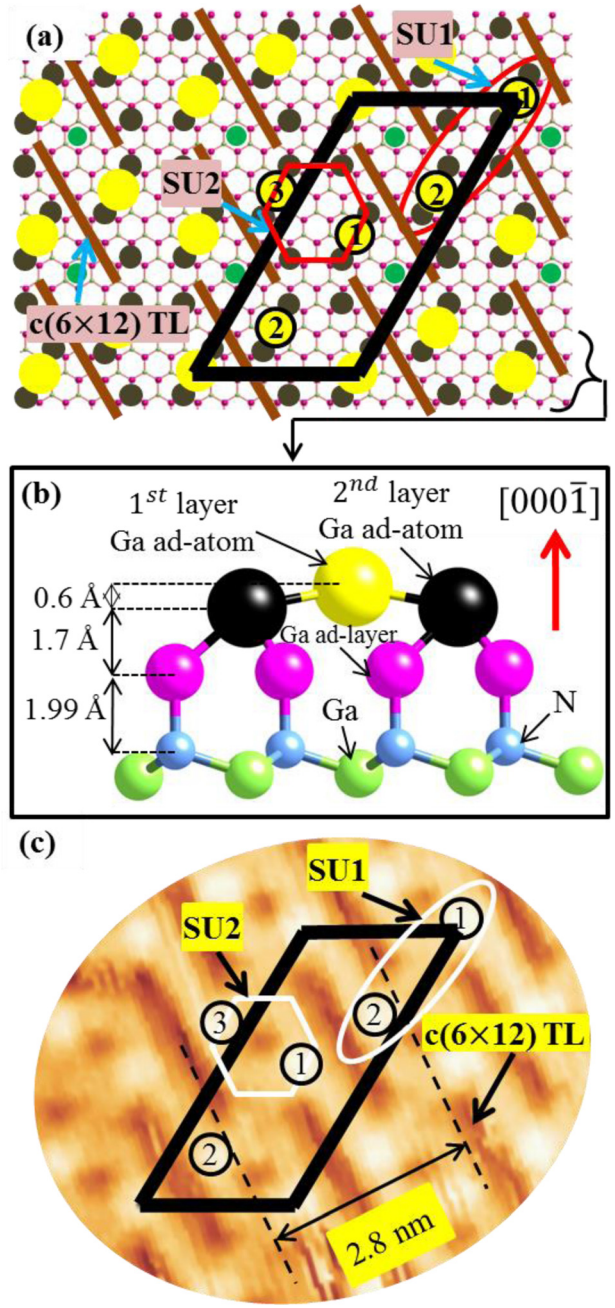

FIG. 4. (Color online) (a) Top view of the c(6 × 12) reconstruction model with SU1 (subunit 1) and SU2 (subunit 2), and c(6 × 12) TL (trench line) indicated; (b) a side view of the c(6 × 12) reconstruction model, with vertical spacings based on measurements from Fig. 3; and (c) STM image of the c(6 × 12) reconstruction. Sample bias $V_S = -1.85$ V, tunnel current $I_T = 51.5$ pA, and scanning speed = 60 nm/s.

Based on the careful comparison of the features of the TLS with the c(6 × 12) structure, we can positively consider the TLS to be an atomic rearrangement of the c(6 × 12), having two characteristic subunits (SUs). It is noted that this is very similar to the Si(001) case in which the 2 × n and 2 × 1 structures are each formed from the same basic subunits—Si dimers. We find here that the WS can be described by a repetition of type 1 SUs, which consist of a pair of the bright dots (atom 1 and atom 2) along with their underlying second layer adatoms. This SU is shown in Figs. 4(a) and 4(c) as SU1 and corresponds exactly to the pair atom 1 + atom 2 shown in Fig. 2(b). The NS can similarly be found to be described excellently using a model built up from repetitions of a type 2 SU. This type 2 SU, labeled in Fig. 4(a) as SU2, is a pair of Ga adatoms and their underlying second layer adatoms correspond to the pair atom 1 + atom 3 in Fig. 2(b). It also corresponds to the Ga adatoms associated with the hexagonal second layer Ga adatom rings shown in Figs. 4(a) and 4(c). The adatom ring and the SU2 subunit are characterized by a dark hole at the center of the ring.

Given the two SUs (SU1 and SU2) as identified by careful comparison of the TLS with the c(6 × 12), one may proceed to build a possible model for the TLS. Possible models for both the WS and the NS are presented in Fig. 5. Figures 5(a) and 5(c) show the top view and the side perspective view models for the WS structure. The WS top view model contains two WSs, which may be directly compared to the zoom-in high resolution STM image of a WS region, as shown in Fig. 5(b). As can be seen, the WS structure consists of a ziz–zag pattern of bright spots bounded on both sides by TLs. From the precise line profile measurement presented in Fig. 3(b), we know that the SU1s must have a spacing along the [11$\bar{2}$0] direction of exactly three primitive GaN units, equal to 9.6 Å.

By placing SU1s in this 3× periodicity, we find a model giving good agreement with the structural features seen in the STM image. This is clearly observed by overlaying an empty circle version of the WS model shown in Fig. 5(a), being composed of SU1's with 3× spacing, directly on top of the STM image in Fig. 5(b). All of the main features seen in the STM image are accounted for in the model. As well,

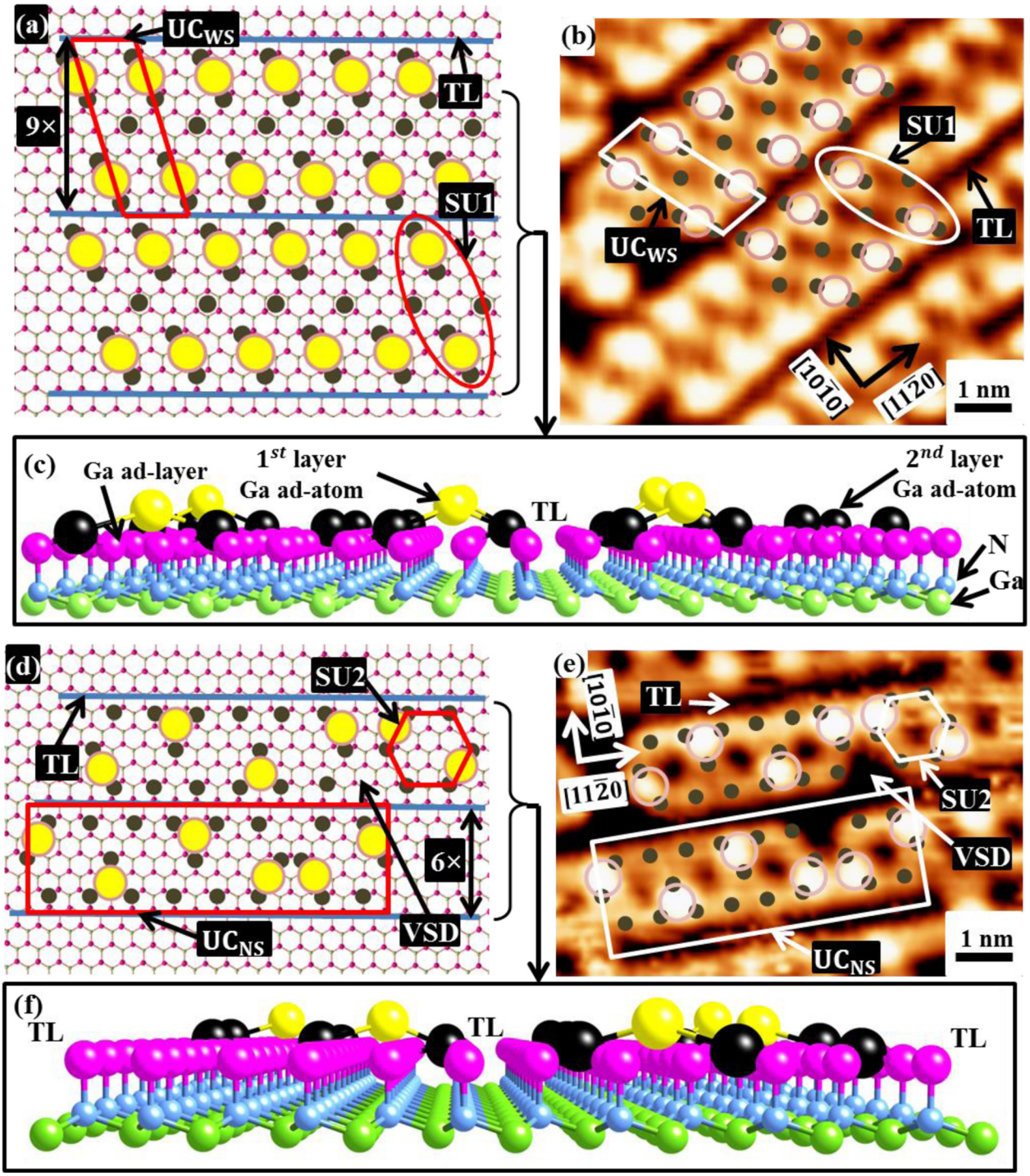

FIG. 5. (Color online) (a) Top view of the TLS-WS model with SU1 (subunit 1) and UC_{WS} (wide strip unit cell), and TL (trench line) indicated; (b) STM image of the TLS-WS with model overlay. Sample bias $V_S = -1.5$ V, tunnel current $I_T = 36.6$ pA, scanning speed = 120 nm/s; (c) a side perspective view of the TLS-WS model; (d) a top view of the TLS-NS model with SU2 (subunit 2) and UC_{NS} (narrow strip unit cell), TL, and VSD (V-shaped defect) indicated; (e) STM image of the TLS-NS with model overlay. Sample bias $V_S = -1.85$ V, tunnel current $I_T = 51.5$ pA, and scanning speed = 60 nm/s; (f) a side perspective view of the TLS-NS model with same atomic labeling as in (c).

from the precise line profile measurements shown in Fig. 3(c), the spacing of TLs is found to be 26 ± 0.5 Å. As seen in the model, this spacing corresponds to 9× periodicity along [10$\bar{1}$0], equal to 9×2.76 Å = 24.8 Å. The TLs in the model of Fig. 5(a) are represented by the horizontal blue lines. The dark TLs correspond to regions where there is a deficiency of second layer atoms, just as with the c(6 × 12). These TLs therefore go down all the way to the gallium adlayer, and the same is the case for the RSDs.

We also observe that the center region of a WS is brighter than the trench lines and RSDs and therefore corresponds to a region containing second layer Ga adatoms. The positions

of these second layer adatoms in the WS model within the center of the strip are adjusted slightly compared to the positions of second layer atoms in the c(6 × 12) model. The second layer adatom number density is similar to the c(6 × 12), but the positions are slightly adjusted to be at the center hollow site and in 3× periodicity.

Shown in Figs. 5(d) and 5(f) is the structural model for the NSs, which is inspired by the close similarity between the hexagonal-like structural subunits (SU2's) seen in the STM images of the NS regions and also in the c(6 × 12) regions. The side perspective view model of the NS structure is shown in Fig. 5(f). It should be noted that just as for the SU1 subunits in the case of the WS model, the crystalline orientation of the hexagonal-like SU2 subunits within the NS model is exactly the same as in the c(6 × 12) model. One important point to note is that the SU2's within the NS model repeat along [11$\bar{2}$0] and sometimes they share a common second layer atom. The positioning of the SU2's within the NS model is determined by careful fitting of these subunits to the STM image, as presented in Fig. 5(e). We find that the prominent protrusions, namely, the Ga adatoms, tend to sit either on their c(6 × 12)-like sites (bridge type sites) or else, in the case where two SU2's are joined by a common second layer atom, on threefold-coordinated sites. Once again, we see the dark hole at the center of the SU2 subunits where there is a lack of second layer adatoms, and in addition, we find characteristic V-shaped defects at the point where two SU2's come together (but do not share a common second layer atom).

V. GALLIUM COVERAGE OF THE TRENCH LINE STRUCTURE

The Ga adatom coverage of the c(6 × 12) structure has been reported in the recent paper by Alam *et al*. as 0.25 ML. It is therefore interesting to measure the Ga adatom coverage for the determined TLS models. Shown in Fig. 5(a) is a unit cell of the repeating WS structure. This unit cell covers an area of 2.38 nm^2, which is also equal to $3 \times 9 = 27$ primitive unit cells. The number of adatoms within the unit cell is 5 (second layer) and 2 (first layer) Ga adatoms. Therefore, the WS Ga adatom coverage is $7/27 = 0.259$, which is slightly higher than the c(6 × 12).

For the NS structural model shown in Fig. 5(d), we can take an average for a large enough unit cell since the structure is not strictly repeating. Taking the rectangular-boxed region as a unit cell, this corresponds to $17 \times 6 = 102$ primitive unit cells with 21 (second layer) and 6 (first layer) Ga adatoms. Therefore, the NS Ga adatom coverage is $27/102 = 0.265$, which is also slightly higher than for the c(6 × 12) and very similar to the WS.

Of course, within a typical surface region, we also find many RSDs. These RSDs contain no Ga adatoms, and therefore, the weighted average Ga adatom coverage for a larger region of the surface containing these defects would be smaller. By forming such a semiperiodic TLS structure, there could be energetic advantages but this would need to be examined theoretically.

VI. CONCLUSIONS

This study examines the formation of trench line structure at the N-polar GaN (000$\bar{1}$) surface, which has been occasionally observed in scanning tunneling microscopy experiments. The nominal sample preparation procedure is the usual one for growing the N-polar GaN surface and achieving the c(6 × 12) structure but then modified through high temperature (800 °C) annealing followed by quenching. The result is that the trench line structure is found at the surface in the vicinity of c(6 × 12) structure. By careful analysis, it is found that the trench line structure, which consists of wide strip and narrow strip regions as well as rectangular shaped defects, has similar structural subunits as the c(6 × 12). Therefore, it turns out to be that models for the wide strip and narrow strip structures can be formed from subunits of the c(6 × 12). The Ga adatom coverages of these two models are found to be only slightly higher than the c(6 × 12). The key to forming these seems to be the high temperature annealing and quenching. We propose that there may be some energetic advantages to forming the extended trench lines; for example, these may lower the energy through some interaction between Ga adatom vacancies. The trench line structure has already been found to be important for the formation of quantum height MnGa islands on N-polar GaN, and it could also be useful for additional applications.

ACKNOWLEDGMENTS

Research has been supported by the U.S. Department of Energy, Office of Basic Energy Sciences, Division of Materials Sciences and Engineering under Award No. DE-FG02-06ER46317. Z.H.A. acknowledges Khan Alam for useful discussions. WSXM software was used for image processing.[29]

[1]S. Nakamura, T. Mukai, and M. Senoh, Appl. Phys. Lett. **64**, 1687 (1994).
[2]S. Nakamura, M. Senoh, S. Nagahama, N. Iwasa, T. Yamada, T. Matsushita, H. Kiyoku, and Y. Sugimotu, Jpn. J. Appl. Phys., Part 2 **35**, L74 (1996).
[3]A. R. Smith, R. M. Feenstra, D. W. Greve, M.-S. Shin, M. Skowronski, J. Neugebauer, and J. E. Northrup, Appl. Phys. Lett. **72**, 2114 (1998).
[4]A. R. Smith, R. M. Feenstra, D. W. Greve, J. Neugebauer, and J. E. Northrup, Phys. Rev. Lett. **79**, 3934 (1997).
[5]A. R. Smith, R. M. Feenstra, D. W. Greve, M.-S. Shih, M. Skowronski, J. Neugebauer, and J. E. Northrup, J. Vac. Sci. Technol., B **16**, 2242 (1998).
[6]A. R. Smith, R. M. Feenstra, D. W. Greve, M.-S. Shin, M. Skowronski, J. Neugebauer, and J. E. Northrup, Surf. Sci. **423**, 70 (1999).
[7]T. Ito, T. Akiyama, and K. Nakamura, J. Cryst. Growth **311**, 3093 (2009).
[8]T. Kawamura, H. Hayashi, T. Miki, Y. Suzuki, Y. Kangawa, and K. Kakimoto, Jpn. J. Appl. Phys., Part 1 **53**, 05FL08 (2014).
[9]N. G. Szwacki, J. A. Majewski, and T. Dietl, Phys. Rev. B **83**, 184417 (2011).
[10]T. Dietl and H. Ohno, Rev. Mod. Phys. **86**, 187 (2014).
[11]E. M. Kneedler, B. T. Jonker, P. M. Thibado, R. J. Wagner, B. V. Shanabrook, and L. J. Whitman, Phys. Rev. B **56**, 8163 (1997).
[12]R. Moosbuhler, F. Bensch, M. Dumm, and G. Bayreuther, J. Appl. Phys. **91**, 8757 (2002).
[13]Y. Qi, G. F. Sun, M. Weinert, and L. Li, Phys. Rev. B **80**, 235323 (2009).
[14]R. Gonzalez-Hernandez, W. Lopez-Perez, M. G. Moreno-Armenta, and J. A. Rodriguez, J. Appl. Phys. **110**, 083712 (2011).
[15]C. Gao, O. Brandt, S. C. Erwin, J. Laehnemann, U. Jahn, B. Jenichen, and H.-P. Schoenherr, Phys. Rev. B **82**, 125415 (2010).
[16]A. Chinchore, K. Wang, M. Shi, Y. Liu, and A. R. Smith, Appl. Phys. Lett. **100**, 061602 (2012).

[17]C. Fowley *et al.*, J. Phys. D: Appl. Phys. **48**, 164006 (2015).
[18]S. Mizukami and A. A. Serga, J. Phys. D: Appl. Phys. **48**, 160301 (2015).
[19]K. Kato, T. Ide, S. Miura, A. Tamura, and T. Ichinokawa, Surf. Sci. **194**, L87 (1988).
[20]H. Niehus, U. K. Kohler, M. Copel, and J. E. Demuth, J. Microsc. **152**, 735 (1988).
[21]J. A. Martin, D. E. Savage, W. Moritz, and M. G. Lagally, Phys. Rev. Lett. **56**, 1936 (1986).
[22]F. K. Men, A. R. Smith, K. J. Chao, Z. Zhang, and C. K. Shih, Phys. Rev. B **52**, R8650 (1995).
[23]A. R. Smith, F. K. Men, K.-J. Chao, and C. K. Shih, J. Vac. Sci. Technol., B **14**, 909 (1996).
[24]H. Luth, *Surfaces and Interfaces of Solid Materials*, 3rd ed. (Springer-Verlag, Berlin Heidelberg, 1995), pp. 35–43.
[25]J. R. Arthur, Surf. Sci. **500**, 189 (2002).
[26]T. Aruga and Y. Murata, Phys. Rev. B **34**, 5654 (1986).
[27]A. R. Smith, R. M. Feenstra, D. W. Greve, J. Neugebauer, and J. E. Northrup, Appl. Phys. A **66**, S947 (1998).
[28]K. Alam, A. Foley, and A. R. Smith, Nano Lett. **15**, 2079 (2015).
[29]I. Horcas, R. Fernndez, J. M. Gmez-Rodrguez, J. Colchero, J. Gmez-Herrero, and A. M. Baro, Rev. Sci. Instrum. **78**, 013705 (2007).